



Published in final edited form as:

*Neuroimage*. 2019 January 01; 184: 359–371. doi:10.1016/j.neuroimage.2018.09.036.

## The alteration landscape of the cerebral cortex

Franco Cauda<sup>a,b,c</sup>, Andrea Nani<sup>a,b,c</sup>, Jordi Manuella<sup>a,b,c</sup>, Donato Liloia<sup>a,b,c</sup>, Karina Tatu<sup>a,b,c</sup>, Ugo Vercelli<sup>a,b,c</sup>, Sergio Duca<sup>a</sup>, Peter T. Fox<sup>d,e</sup>, Tommaso Costa<sup>a,b,c</sup>

<sup>a</sup>GCS-fMRI, Koelliker Hospital and Department of Psychology, University of Turin, Turin, Italy

<sup>b</sup>Department of Psychology, University of Turin, Turin, Italy

<sup>c</sup>FOCUS Lab, Department of Psychology, university of Turin, Turin, Italy.

<sup>d</sup>Research Imaging Institute, University of Texas Health Science Center at San Antonio, USA

<sup>e</sup>South Texas Veterans Health Care System

### Abstract

Growing evidence is challenging the assumption that brain disorders are diagnostically clear-cut categories. Transdiagnostic studies show that a set of cerebral areas is frequently altered in a variety of psychiatric as well as neurological syndromes. In order to provide a map of the altered areas in the pathological brain we devised a metric, called alteration entropy (A-entropy), capable of denoting the “structural alteration variety” of an altered region. Using the whole voxel-based morphometry database of BrainMap, we were able to differentiate the brain areas exhibiting a high degree of overlap between different neuropathologies (or high value of A-entropy) from those exhibiting a low degree of overlap (or low value of A-entropy). The former, which are parts of large-scale brain networks with attentional, emotional, salience, and premotor functions, are thought to be more vulnerable to a great range of brain diseases; while the latter, which include the sensorimotor, visual, inferior temporal, and supramarginal regions, are thought to be more informative about the specific impact of brain diseases. Since low A-entropy areas appear to be altered by a smaller number of brain disorders, they are more informative than the areas characterized by high values of A-entropy. It is also noteworthy that even the areas showing low values of A-entropy are substantially altered by a variety of brain disorders. In fact, no cerebral area appears to be only altered by a specific disorder. Our study shows that the overlap of areas with high A-entropy provides support for a transdiagnostic approach to brain disorders but, at the same time, suggests that fruitful differences can be traced among brain diseases, as some areas can exhibit an alteration profile more specific to certain disorders than to others.

---

Corresponding author: Franco Cauda, Department of Psychology, Via Po 14, 10123 Turin, Italy, franco.cauda@unito.it.

Authors' contributions

FC conceived the experiment, supervised data collection, analyzed the data, drafted and revised the article. AN, JM, KT and UV drafted and revised the article. DL implemented data collection, organized the dataset, retrieved information of the sampled population, drafted, and revised the article. SD and PF revised the article. TC devised the tools for the analyses, analyzed the data, drafted, and revised the article.

**Publisher's Disclaimer:** This is a PDF file of an unedited manuscript that has been accepted for publication. As a service to our customers we are providing this early version of the manuscript. The manuscript will undergo copyediting, typesetting, and review of the resulting proof before it is published in its final citable form. Please note that during the production process errors may be discovered which could affect the content, and all legal disclaimers that apply to the journal pertain.

Declaration of interests

The authors declare no competing interests.

## Keywords

Brain disorders; Brain alterations; Voxel-based morphometry; Alteration entropy; Brain networks

---

## 1. Introduction

The analysis of the cerebral areas that appear to be co-altered in brain disorders can provide invaluable insights for better understanding these diseases. This approach is especially important with regard to mental illnesses, as it could radically improve their classification as well as their diagnoses (Hyman, 2010). The DSM-based models of psychopathology (American Psychiatric Association, 2013) and the corresponding categorization of the World Health Organization (World Health Organization, 2007) treat psychiatric disorders as distinct pathological constructs with different etiologies and biomarkers. However, this view (derived from clinical observations and patient self-reports) is likely to be mistaken. On the one hand, traditional classifications may consider to be similar certain clinical manifestations that are instead characterized by biological heterogeneity; on the other hand, these classifications may categorize as different certain diseases that might share neurobiological underpinnings.

This diagnostic rigidity has stirred the idea that each defined disorder is real, clear-cut and caused by specific factors, but increasing evidence is beginning to challenge this assumption (Buckholtz and Meyer-Lindenberg, 2012). For instance, large-scale phenotypic studies show that brain disorders have common liabilities and that the acute manifestation of symptoms does not exactly correspond to noticeable deficits in cognitive functions (Buckholtz and Meyer-Lindenberg, 2012; Krueger, 1999). Comorbidity, too, is a sign that defies a rigid classification, especially of mental disorders. Indeed, the clinic picture of co-occurrences of psychiatric diseases is rather the rule than the exception. The co-variation between diagnoses of mental disorders is so common that makes the categories described in our clinical manuals very artificial. Thus, this broad variability in symptomatology, dimensionality and comorbidity (Kessler et al., 2005; Krueger and Markon, 2011; Markon, 2010) suggests that our categorical models need profound revision (Krueger and Markon, 2006).

Etiological studies provide further support for discarding any rigid categorization of mental illnesses, which are frequently characterized by polygenic inheritance with multiple small-effect risk alleles that bring about a continuous distribution of genetic liability (Gejman et al., 2011). Moreover, with regard to psychiatric disorders, the genetic risk is pleiotropic, thus capable of impacting on broad dimensions of symptomatically-related conditions – see the case of bipolar disorder and schizophrenia (Gejman et al., 2011; Purcell et al., 2009). This complex etiological picture implies that mental illnesses might be extreme expressions of quantitative traits that are generally distributed throughout the population (Plomin et al., 2009), and challenges our traditional categorical models based on closed symptomatic domains.

From the clinical point of view, similar considerations hold true for neurological diseases as well. In particular, differential diagnosis between types of neurodegenerative conditions – for instance, mild cognitive impairment, Alzheimer's disease (AD) and frontotemporal lobar

degeneration – is often challenging (Bird and Smith , 2018; Padovani et al., 2013). Several biomarkers, such as amyloid- $\beta$  (A $\beta$ ) plaques, neurofibrillary tangles and other pathological deposits, have been proposed to differentiate these types of disorders. To date, however, for the cases characterized by high uncertainty only the autopsy can confirm or reject the clinical diagnosis. And similar to psychiatric conditions recent research has proposed models of alteration spread based on network-like patterns (Iturria-Medina and Evans, 2015; Raj et al., 2012; Seeley et al., 2009).

This new trend in considering brain disorders is supported by transdiagnostic studies showing that a common set of cerebral areas is frequently altered in a variety of psychiatric conditions (Buckholtz and Meyer-Lindenberg, 2012; Cauda et al., 2017; Cauda et al., 2018; Cole et al., 2014; Goodkind et al., 2015; McTeague et al., 2016). These studies suggest that the investigation of brain disorders under the aspect of their common alteration patterns is extremely useful, as it can provide an essential bridge between neurobiology and clinical practice.

The present study aims to start building one of the pillars of this bridge by analyzing how each cerebral area is altered by a great or small number of brain disorders and by identifying whether or not certain areas are typically more vulnerable to specific diseases. To do so we decided to use the whole disease-related voxel-based morphometry (VBM) database of BrainMap ([www.brainmap.org](http://www.brainmap.org)) (Fox et al., 2005; Fox and Lancaster, 2002; Laird et al., 2005b). BrainMap is an online open access database which applies a systematic coding scheme; it contains over 15000 published human neuroimaging experimental results and reports over 120000 brain locations in stereotactic space. Its VBM dataset constitutes therefore an ideal environment for conducting structural meta-analyses (Fox et al., 2005; Fox and Lancaster, 2002; Laird et al., 2005b; Vanasse et al., 2018). VBM is a computational procedure that can measure focal differences in the concentration, density or volume of brain tissues between healthy and pathological subjects (Ashburner and Friston, 2000). We retrieved from BrainMap all the data that were stored in its VBM database regarding brain diseases, so as to achieve the most overarching investigation of how neuropathological processes affect the brain.

In order to understand how morphometric alterations differentiate within each cerebral area we devised a metric, which we have called “alteration entropy” or A-entropy, based on Shannon’s entropy, capable of denoting the “structural alteration variety” of an altered region. This type of analysis has already been used in functional contexts by Anderson et al. (2013), but so far it has never been applied to the study of morphometric alterations. The metric of A-entropy is based on the idea that the measurement of structural varieties is similar to the measurement of the informational content in a message; it therefore makes possible to identify the brain areas exhibiting a high degree of overlap between neuropathologies (or high value of A-entropy) and those exhibiting a low degree of overlap (or low value of A-entropy; this can also be mathematically defined as high value of A-negentropy, which is the reverse of the A-entropy, see Liloia et al. (submitted) for more details). As a result, the former areas are supposed to be more vulnerable to a variety of brain diseases, while the latter are supposed to be more informative about the impact of specific brain diseases.

## 2. Materials and methods

### 2.1 Selection of studies

Analyses were performed on the whole VBM dataset of BrainMap until March 2016. Data have been previously codified by the BrainMap staff on the basis of the International Statistical Classification of Diseases and Related Health Problems, release 10 (ICD-10). The dataset included 646 studies, 1827 experiments, 19325 subjects and 20238 foci of gray matter (GM) decrease/increase (see Liloia et al. (submitted) for further information). For each eligible experiment stored in the VBM dataset, the BrainMap staff provided us with the categorical class (ICD pathological block) of the sample with the relative alphanumeric code, as well as with the specific alphanumeric code of the single pathological condition (ICD pathological category). This allowed us to carry out our analyses both on the coarse-grained subdivision and on the fine-grained subdivision of the ICD-10. At the time of the selection of studies, the VBM dataset consisted of 40 ICD pathological blocks, for a total of 82 ICD pathological categories.

Differently from what our team and another research group did in previous works, which were focused only on psychiatric diseases (Cauda et al., 2017; Cauda et al., 2018; Goodkind et al., 2015), in this study we included all the brain disorders stored in BrainMap. We did so because we were interested in investigating in a more comprehensive way the overlaps between all the alteration patterns induced by neuropathological processes. Moreover, during a pilot inspection of the BrainMap database, we had found that overlaps between brain alterations were not confined to psychiatric conditions but largely included neurological disorders as well. This does not obviously suggest that, contrary to Crossley et al. (2015), psychiatric and neurological diseases are not dissociable on the basis of neuroimaging evidence, but, at least, puts forward the intriguing possibility that categorically different neuropathological processes might in part exhibit common patterns of neuronal alterations.

### 2.2 Anatomical likelihood estimation and creation of modeled activation maps

We first performed an anatomical likelihood estimation (ALE) (Eickhoff et al., 2012; Eickhoff et al., 2009; Turkeltaub et al., 2012) using an in-house developed Matlab<sup>®</sup> script following both the algorithms utilized in Gingerale 2.3.6 and the recommendation of Eickhoff et al. (2017). Results have been clustered at a level of  $p < 0.05$ , family-wise error-corrected for multiple comparisons, with a cluster-forming threshold of  $p < 0.001$  at voxel level. The ALE is a quantitative voxel-based meta-analysis technique able to give information about the anatomical reliability of results through a statistical comparison, using a sample of reference studies from the existing literature (Laird et al., 2005a).

An ALE meta-analysis models each focus of every experiment as a Gaussian probability distribution:

$$p(d) = \frac{1}{\sigma^3 \sqrt{(2\pi)^3}} e^{-\frac{d^2}{2\sigma^2}}$$

where  $d$  is the Euclidean distance between the voxels and the focus taken into account, and  $\sigma$  is the spatial uncertainty.

Then for each experiment a modeled alteration (MA) map was calculated as the union of the Gaussian probability distribution of each focus of the experiment. The union of the MA maps resulted in the final ALE map.

The significance of the ALE map activations was assessed by a permutation test that redistributed the same number of foci in the brain and calculated an ALE map as described before. Finally, the histogram of the obtained scores was used to assign a threshold for P values. For calculating the A-entropy metric we used the unthresholded ALE map of every brain disorder so as to obtain for each brain area the probability distribution of its alteration.

### 2.3 A-Entropy

In the literature, entropy has been used as measure of diversity, complexity and randomness in different contexts, from economics to biology. If we define the informational content of an event  $x$  as:

$$I = \log_b p(x)$$

where  $b$  is the base of the logarithm (usually base 2), then, the entropy  $H$  of a discrete random variable  $X$  with values  $\{x_1, x_2, \dots, x_n\}$  and probability  $P(X)$  is defined as:

$$H(X) = E[-\log_b P(X)]$$

In our case, from each ALE thresholded map of every brain disorder we calculated the probability of every brain disorder  $p_i$  and the entropy in each voxel as:

$$H_j = - \sum_i p_{ij} \ln(p_{ij})$$

where  $p_{ij}$  is the probability of the voxel  $j$  in the brain disorder  $i$ .

To get comparisons relative to the number of brain disorders we also used the normalized A-entropy, which is determined as follows. Given the A-entropy of each voxel calculated with the previous formula, the result is divided by the A-entropy obtained considering a uniform distribution of probability of the brain disorders:

$$p_{ij} = \frac{1}{N}$$

so that the maximum A-entropy is

$$H_{\max} = \ln N$$

We thus obtain a relative metrics showing the degree of homogeneity of the distribution of brain disorders in the voxel considered. This is a robust and representative metric because it is true for any value of N.

## 2.4 Network decompositions

In a previous study by Biswal et al. (2010) the brain surface was parcellated using a large cohort of volunteers (1414) who underwent a resting-state fMRI scan. Authors found out that, on the basis of data-driven methodology, 20 large-scale networks could be identified within the brain at rest; these networks are also recognizable when the brain is performing a task. Following the Biswal's parcellation, we determined the mean ALE values of the GM voxels included in each of the following networks: premotor (PreMOT), dorsal attentional (DAN), orbitofrontal (OFC), ventral attentional right and left (VAN R and L), thalamus and basal ganglia (TH-Ganglia), default mode network (DMN), salience, motor, sensorimotor (SensMOT), cerebellum, auditory, V1, V2 and V3 (Fig. 1, middle panel).

## 2.5 Winner takes all and overlap maps

To compare the alteration map and the A-entropy map we performed two analyses:

- 1) A winner takes all map (WTA). To calculate this map we employed the normalized alteration probability map (normalized unthresholded ALE map) and the normalized A-entropy map. We attributed to each voxel a value of 0 or 1 according to its prevalent involvement into the ALE map or the A-entropy map. To visualize the WTA map we assigned the color blue to the areas in which values of A-entropy were prevalent and the color red to the areas in which values of ALE were prevalent.
- 2) An overlap map. To calculate this map we employed the thresholded ALE map (see Methods) and we thresholded the A-entropy map by setting to zero all the voxels with values  $<0.5$ . To visualize this map we assigned the color green to the areas of overlap and the color red to the areas with only A-entropy values. No areas with only ALE values were found.

## 3. Results

### 3.1 A-Entropy

An important finding of our analysis is that there are no brain areas affected by just one brain disorder. Indeed, most of the brain areas appear to be altered by the majority of the diseases taken into consideration in this study (see Table 2 in Liloia et al. (submitted) for a detailed description of this result).

The upper and lower panels of Figure 1 show 2D and 3D visualizations of the A-entropy calculated using a fine-grained neuropathological subdivision (ICD pathological categories). As we have already said, the A-entropy metric (Shannon, 1948) can express the variety of neuropathologies causing structural alteration (Magurran, 2004) exhibited by a brain region. As detailed in Table 1, several brain areas are characterized by high values of A-entropy. The areas with the highest peak values (i.e., the maximum normalized A-entropy) are the

following: right anterior insula, left precentral gyrus, left inferior temporal gyrus, left medial frontal gyrus, right caudate head and right anterior cingulate. Instead, the areas with the highest mean values (i.e., the mean normalized A-entropy) are the following: the amygdalae, the medial dorsal nucleus of the thalamus, the hippocampi, the left and right anterior insula and the parahippocampal gyri.

The middle panel of Figure 1 shows that the large-scale brain networks with the highest A-entropy rates are mainly the more integrative ones, encompassing ventral and dorsal attentional/executive, orbitofrontal, emotional, salience, thalamus/basal ganglia, default mode and premotor networks. On the contrary, the visual (V1, V2, V3), auditory, cerebellar and sensorimotor networks exhibit lower A-entropy rates (see Table 1 for more details about the maximum and the mean A-entropy values for each brain area; interestingly, certain brain areas have high both the maximum and mean values, while others have low mean values even though some of their peaks exhibit high maximum values, which means that the A-entropy distribution is less uniform).

Figure 2 shows a comparison between the A-entropy calculated on the basis of a fine-grained neuropathological subdivision (ICD pathological categories, Fig. 2 upper panel first row) and the A-entropy calculated on the basis of a coarser subdivision (ICD pathological blocks, Fig. 2 upper panel second row). Not surprisingly, the fine-grained subdivision leads to a more entropic map but, interestingly, both maps showed the aforementioned areas to be the ones with the highest A-entropy. These cerebral areas are altered in almost all the brain disorders considered in this study (see also Table 1 and 2 in Liloia et al. (submitted)). The middle panel of Figure 2 shows the ALE map of all the disease-related GM alterations detected with VBM and included in the BrainMap database. The areas showing high values of A-entropy are often the areas that are more frequently altered in the ALE map (however, this is not always the case: there are in fact various regions with high A-entropy showing low p values in the alteration ALE map). This may seem an expected result, as areas that mostly overlap between brain disorders are also the more susceptible to be altered. However, on further reflection this result is intriguing, as the algorithm employed for calculating the A-entropy normalizes the results on the basis of the number of alterations found in each voxel, so that the “overlapping effect” should be removed.

### 3.2 Winner takes all and overlap maps

The two lower panels of Figure 2 shows comparisons between the ALE and the A-entropy maps (fine-grained). One panel (the row before last) shows the WTA map between normalized probabilities of alteration and A-entropy. The areas characterized by an A-entropy prevalence are located in sensorimotor/premotor, angular, dorsolateral prefrontal, superior temporal districts and posterior parietal gyri.

The other panel (the last row) shows the overlap map between alteration and A-entropy. Regions with high A-entropy but not frequently altered (and thereby not overlapping with significant areas in the ALE map) are highlighted in red. Notably, these regions (pertaining to dorsolateral prefrontal, sensorimotor/premotor, posterior parietal, superior temporal districts and angular gyri) cover most of the areas with high A-entropy that are not parts of the salience network; instead, they are mainly parts of the executive network. The areas

highlighted in green are those of overlap between the ALE map and the A-entropy map. These regions principally pertain to the salience and the default mode networks. No areas showing significant ALE results and low A-entropy values are revealed.

Since a very high percentage of alterations seems to affect the insulae, we decided to analyze the A-entropy patterns within these brain areas and comparing those patterns to the ALE results. Figure 3 shows that the insular portions with the highest A-entropy values are the anterior insula along with a superior layer extending through the mid-posterior insula. The ALE map shows a very similar pattern.

The fact that the alteration probability maps (i.e., the unthresholded ALE map) and the A-entropy maps overlap greatly in some areas is not an obvious result. To better understand the point, let us see in more detail how the final ALE map is obtained.

If we have  $n_i$  experiments for  $k$  neuropathologies, then  $N = \sum_{i=1}^k n_i$ . For each experiment we calculate the probability of activation of every voxel, as follows:

$$L_i(v) = \frac{1}{\sigma^3 \sqrt{(2\pi)^3}} e^{-\frac{d^2}{2\sigma^2}}$$

For all the experiments the resulting ALE is then:

$$ALE(v) = 1 - \prod_{i=1}^N (1 - L_i(v))$$

The final ALE is therefore the product of the ALE values of each considered experiment. As the calculation is commutative for the single values, this formula collapses the information regarding the different neuropathologies, so that it is not possible to infer the contribution to the map of a specific brain disorder. In contrast, when we consider the A-entropy values we can obtain a map for each brain disorder. All the A-entropy values are in fact normalized to obtain a probability distribution of neuropathologies. This distribution is then used in the A-entropy calculation and, as a consequence, the information contained in the A-entropy map is different from the one contained in the ALE map. In fact the A-entropy weighs the contribution of each brain disorder that is present in the probability distribution.

The high values of the ALE map indicate only that we have a high probability of activation regardless of the type of brain disorder. In contrast, the high values of the A-entropy map indicate that the probability of activation is really high for many neuropathologies. The two maps are therefore complementary and both the similarity and dissimilarity that certain areas show in the two maps (see the last panel of Fig. 2) provide relevant information.

### 3.3 Core areas

In a previous study (Cauda et al., 2012b) we showed how certain brain areas (including the anterior insulae, the thalami and the cingulate cortices) are activated by a wide range of cognitive tasks, encompassing pain, memory, touch, interoception, attention, action,

emotion, and reward. Most of these “core areas” are important parts of the cognitive control system (Cole et al., 2014; McTeague et al., 2016; Miyake and Friedman, 2012) and because of their intense functional connectivity are thought to be more vulnerable to neuropathological processes (Cauda et al., 2017; Cauda et al., 2018; Cauda et al., 2012b; Cauda et al., in press; Crossley et al., 2014; Manuello et al., 2018; Tatu et al., 2018; Zhou et al., 2012).

We were therefore interested in investigating whether or not these core areas may be characterized by high entropy values and, thereby, be part of a “high A-entropy group”. Figure 4 shows a comparison between the two source maps (for a tridimensional view of the same results see also the green areas showed in the lower panel of Figure 2). Of note, the core areas (Cauda et al., 2012b) show a relevant overlap with the highest entropic brain areas. It is also interesting to note that the areas with low values of A-entropy are quite similar to the areas that in Cauda et al. (2012b) were found to exhibit a low percentage of overlap (for a detailed description of low A-entropy areas see Liloia et al. (submitted)).

These findings suggest that the brain areas involved in a great variety of cognitive tasks are typically more characterized by high A-entropy values. Moreover, this observation is partially confirmed by the results of Anderson et al. (2013), which provide evidence that certain areas (distributed in prefrontal, insular, cingulate, thalamic and premotor cortices) show a high diversity of activation (i.e., high functional entropy) in different cognitive tasks.

#### 4. Discussion

In this study we analyzed the “structural alteration variety” (Magurran, 2004) of brain areas. To do so we have devised the A-entropy metric capable of indicating how brain areas are differentiated in terms of their alteration profiles based on their A-entropy values (Shannon, 1948). Cerebral areas with high values of A-entropy are affected by a large number of brain disorders; they are therefore little informative and have a limited predictive power about the neuropathological processes to which they are vulnerable. On the other hand, cerebral areas with low values of A-entropy are altered by a small number of brain disorders, so that they may be more informative about the nature of the disease and its development.

Our analysis points out that areas with low values of A-entropy are sparse, even though they tend to concentrate in brain sites with unimodal functions, in particular in the visual regions. In contrast, several areas, especially those involved in networks with cognitive and integrative functions, are highly entropic, which means that they are altered by a large number of brain disorders. In fact, the great variety of cognitive, social and emotional activities that shape the human lives are supported by the interaction of large-scale brain networks, which can be disrupted by different types of neuropathological processes (Crossley et al., 2014; Seeley et al., 2009).

Among the highly entropic areas the insula exhibits the highest values of maximum and of mean normalized A-entropy (Cauda et al., 2012a; Cauda et al., 2011). Specifically, its anterior and, to some extent, medial parts are associated with the salience network, as well as with the DMN (Mohan et al., 2016) and with the dorsal and ventral attentional networks

(Vercelli et al., 2016). The anterodorsal region underpins cognitive, salience and decision making functions associated with the cognitive control system, while the anteroventral region is involved in emotional and autonomic regulation (Bauernfeind et al., 2013; Chang et al., 2013; Christopher et al., 2014; Craig, 2002; Singer et al., 2009).

If we compare the areas with high A-entropy values with the areas that appear to be the most frequently altered by brain disorders (i.e., showing high ALE values), we see that the former mostly overlap with the latter, especially with regard to subcortical and cingulate/insular regions. However, other areas, located especially in frontoparietal and temporal regions, do not appear to be frequently altered, even though they are characterized by high A-entropy values.

Of note, areas with high A-entropy mostly overlap with areas exhibiting a wide differentiation in their functional activations (Anderson et al., 2013); they have, in other words, a high functional entropy. As we have already pointed out, these regions have been identified as parts of a set of core areas that is involved in a variety of cognitive functions. This set comprises highly connected cortical hubs (Achard et al., 2006), which have been found to be typically altered by brain disorders (Crossley et al., 2014).

Quite recently, an interesting model has been put forward by Buckholtz and Meyer-Lindenberg (2012) to explain this complex picture (see Fig. 5 for a diagram illustrating this model). According to these authors the breakdown of the interaction between networked brain areas is capable of producing a panoply of cognitive and affective symptoms, which are transdiagnostically shared by different diseases. So, the more disrupted the large-scale networks are, the more diversified is the susceptibility to neuropathological conditions. The involvement of these core areas in the pathological brain affects several dimensions of cognition and, thereby, causes vulnerability to broad domains of neuropathology rather than to specific disorders. This is why similar patterns of disconnectivity are observed across multiple diagnostic boundaries (Goodkind et al., 2015) and, as we said above, explains the fact that comorbidity between brain disorders appears to be generally the case.

With regard to the genetic point of view, the pleiotropic risk associated with genes appears to increase susceptibility to a variety of brain disorders. For instance, twin studies show that common genetic factors can mostly account for clusters of syndromes (Wen et al., 2016), thus suggesting a biological basis for comorbidity (Kendler et al., 2011; Kendler et al., 2003). Indeed, high covariation at the phenotypic level appears to be influenced by high covariation at the genetic level (Lahey et al., 2011). According to this view, patterns of genetic covariance across individual genomes would lead to patterns of covariance in connectivity profiles and, as a consequence, bring about patterns of symptoms' covariance (i.e., comorbidity). In other words, the overt constellations of different symptoms in psychopathological conditions may partly reflect a genetically-determined latent structure of brain connectivity.

Our analysis supports the model proposed by Buckholtz and Meyer-Lindenberg (2012), as it shows that certain areas are generally altered in a wide range of diseases (see the upper panels of Figures 1 and 2). Moreover, brain networks do not appear to be all equally

involved. Networks associated with cognitive functions, such as the salience network, the dorsal and ventral attentional networks and the DMN exhibit higher values of A-entropy. So far, studies have highlighted that the cognitive control system (Cole and Schneider, 2007) is one of the most involved circuits in psychopathology (Buckholtz and Meyer-Lindenberg, 2012; Caspi et al., 2014; Cole et al., 2014; McTeague et al., 2016). Our findings support this hypothesis but, in addition to the cognitive control system – which is divided in subunits by our independent component analysis (Esposito and Goebel, 2011) on large-scale brain networks used as regions of interest (ROIs) – suggest that other important functional systems may play a relevant part in the clinical picture of the pathological brain, especially when subcortical areas are involved. The overemphasis on the cognitive control system may be due to the fact that the aforementioned studies limited the scope of their analyses on psychiatric diseases instead of focusing, as we did, on a broader range of conditions.

The attempt to pinpoint common neurobiological roots among brain disorders, which could serve as transdiagnostic links, is synergistic with current efforts to redefine psychiatric nosology in terms of underlying biology, such as the Research Domain Criteria (RDoC) initiative of NIMH (Insel, 2014). However, while RDoC is organized around domains that roughly correspond to neuropsychological functions, the idea proposed by Buckholtz and Meyer-Lindenberg (2012) goes one step further, as it proposes that specific circuits should be thought of as meaningful systems-level units of inquiry in order to both investigating etiology and transdiagnostic underpinnings.

These approaches do not imply that phenotypic differences between diagnoses are supposed to be negligible. In fact, disruption in large-scale networks with highly integrative and associative functions does not preclude the manifestation of distinct deficits related to specific disorders as well as to specific brain areas. Indeed the analysis of the low A-entropy areas can be seen as the other side of the coin with respect to the transdiagnostic pattern of brain A-entropy.

On the basis of the pattern of brain alterations, low A-entropy areas appear to be the most informative for diagnostic purposes; in fact, being altered by a few diseases, they allow a better identification of the pathological processes affecting the brain, especially if their alteration occurs in the early stages of the disease. This would also be significant information for an in-depth understanding of the pathological brain, as it would help reduce and better define the number of potential pathological causes of the alterations.

An interesting result of our analysis is that no brain area can be deemed immune to pathological alterations. In principle, every area of the cortex can be more or less vulnerable to several pathological processes; and this can lead to a great overlap of alterations caused by different brain disorders. This result, however, is not completely unexpected, as it may be partly due to the severity and stage of disease development included in BrainMap. During their last stages, in fact, many disorders will eventually affect large portions of the brain. What differentiates a brain disease from the others, then, is whether or not it affects areas with low A-entropy, as well as its early stages (i.e., areas of pathological inception) and its typical spatial progression.

The two analyses carried out in this study (i.e., the ALE and the A-entropy calculations), therefore, provide an overarching picture of the pathological brain, which is of great interest for a better understanding of how neuropathological processes can affect this organ. Intriguingly, though a large number of brain areas appear to be altered by the majority of diseases, profiles of alterations specificity to certain neuropathological conditions may still emerge, so as to give rise to the diversified landscape of structural alteration variety. These peculiarities are valuable insights that can help us improve our clinical tools for better predicting the development of brain disorders.

#### 4.1 Limitations and future directions

Since the BrainMap database used for this study does not report for each disease an equal number of experiments, our results do not represent equally all the disorders taken here into consideration. Furthermore, the use of meta-analytic data, which are characterized by a certain degree of deterioration and of spatial uncertainty, may have enhanced the overlap between areas affected by different brain disorders and, thereby, partly increased their values of A-entropy. However, we believe that the good levels of overlaps found in this study describe real phenomena, as they can be determined only residually by the spatial uncertainty of meta-analytic data. Relationships between the entropic values of brain areas are in no way supposed to be influenced by these issues.

Future investigations could be based on a tool (working on the VBM disease-related data of BrainMap) that allows the inverse Bayesian inference so as to verify how informative are the low A-entropy areas about the pathological impact of brain disorders. Furthermore, A-entropy maps could serve for comparisons in meta-analytic studies with alteration patterns of specific disorders or categories of diseases. With regard to this, we aim to provide the BrainMap database with our maps, so that other researchers could use them to compare alteration patterns associated with specific disorders or categories, or to select ROIs for specific investigations.

## 5. Conclusion

This study has investigated how a large number of brain disorders can preferentially cause patterns of structural alterations to few specific brain areas. The A-entropy is a valuable metric capable of denoting the “structural alteration variety” of an altered region. Our analysis shows that regions characterized by high values of A-entropy are multimodal/polymodal and are, therefore, frequently parts of large-scale brain networks associated with cognitive/integrative functions. Coherently, unimodal areas exhibit less overlap and are characterized by low values of A-entropy.

These findings provide support for a transdiagnostic model suggesting that genetic and environmental risk factors can disrupt patterns of interaction between brain regions and, as a consequence, increase the vulnerability to neuropathology. The disruption of brain circuits supporting multiple cognitive processes may lead to deficits and symptoms related to specific cognitive domains with an overlap of diagnostic taxa. In a sense, certain symptoms could constitute diagnostic criteria for disorder “A” but not for disorder “B” and, conversely, certain other symptoms could be to some extent selective for disorder “B” but not for

disorder “A”. Overall, however, taken as a whole, this plurality of symptoms is likely to be associated with a transdiagnostic feature of brain disorders that are traditionally considered as separate clinical entities, given that at their root the neurobiological underpinnings are the same.

The identification of low A-entropy areas put forward by this study may serve as clinical and experimental insights in order to better understand distinctions and similarities between brain disorders. Our study shows that the overlap of brain areas with high A-entropy provides support for a transdiagnostic view of neuropathological processes but, at the same time, especially through the analysis of the low A-entropy patterns, suggests that fruitful differences can be traced among brain diseases. These findings open interesting prospects for better characterizing brain disorders, thus hopefully contributing to the intriguing endeavor to decipher the complex alteration landscape of the pathological brain.

## Acknowledgments

Funding: This study was supported by the Fondazione Carlo Molo (F Cauda, PI), Turin, NIH/NIMH grant MH074457 (P Fox, PI) and CDMRP grant W81XWH-14-1-0316 (P Fox, PI).

## References

- Achard S, Salvador R, Whitcher B, Suckling J, Bullmore E, 2006. A resilient, low-frequency, small-world human brain functional network with highly connected association cortical hubs. *J Neurosci* 26, 63–72. [PubMed: 16399673]
- American Psychiatric Association, 2013. *Diagnostic and Statistical Manual of Mental Disorders, Fifth Edition (DSM-5)*, 5th, ed. American Psychiatric Publishing, Arlington, VA.
- Anderson ML, Kinnison J, Pessoa L, 2013. Describing functional diversity of brain regions and brain networks. *Neuroimage* 73, 50–58. [PubMed: 23396162]
- Ashburner J, Friston KJ, 2000. Voxel-based morphometry--the methods. *Neuroimage* 11, 805–821. [PubMed: 10860804]
- Bauernfeind AL, de Sousa AA, Avasthi T, Dobson SD, Raghanti MA, Lewandowski AH, Zilles K, Semendeferi K, Allman JM, Craig AD, Hof PR, Sherwood CC, 2013. A volumetric comparison of the insular cortex and its subregions in primates. *J Hum Evol* 64, 263–279. [PubMed: 23466178]
- Bird TD, Smith CO, 2018. Clinical approach to the patient with neurogenetic disease. *Handb Clin Neurol* 147, 3–9. [PubMed: 29325619]
- Biswal BB, Mennes M, Zuo XN, Gohel S, Kelly C, Smith SM, Beckmann CF, Adelstein JS, Buckner RL, Colcombe S, Dogonowski AM, Ernst M, Fair D, Hampson M, Hoptman MJ, Hyde JS, Kiviniemi VJ, Kotter R, Li SJ, Lin CP, Lowe MJ, Mackay C, Madden DJ, Madsen KH, Margulies DS, Mayberg HS, McMahon K, Monk CS, Mostofsky SH, Nagel BJ, Pekar JJ, Peltier SJ, Petersen SE, Riedl V, Rombouts SA, Rypma B, Schlaggar BL, Schmidt S, Seidler RD, Siegle GJ, Sorg C, Teng GJ, Veijola J, Villringer A, Walter M, Wang L, Weng XC, Whitfield-Gabrieli S, Williamson P, Windischberger C, Zang YF, Zhang HY, Castellanos FX, Milham MP, 2010. Toward discovery science of human brain function. *Proc Natl Acad Sci U S A* 107, 4734–4739. [PubMed: 20176931]
- Buckholtz JW, Meyer-Lindenberg A, 2012. Psychopathology and the human connectome: toward a transdiagnostic model of risk for mental illness. *Neuron* 74, 990–1004. [PubMed: 22726830]
- Caspi A, Houts RM, Belsky DW, Goldman-Mellor SJ, Harrington H, Israel S, Meier MH, Ramrakha S, Shalev I, Poulton R, Moffitt TE, 2014. The p Factor: One General Psychopathology Factor in the Structure of Psychiatric Disorders? *Clin Psychol Sci* 2, 119–137. [PubMed: 25360393]
- Cauda F, Nani A, Manuella J, Premi E, Palermo S, Tatu K, Duca S, Fox PT, Costa T, in press, Brain structural alterations are distributed following functional, anatomic and genetic connectivity. *Brain*

- Cauda F, Costa T, Nani A, Fava L, Palermo S, Bianco F, Duca S, Tatu K, Keller R, 2017. Are schizophrenia, autistic, and obsessive spectrum disorders dissociable on the basis of neuroimaging morphological findings?: A voxel-based meta-analysis. *Autism Research*, n/a-n/a.
- Cauda F, Costa T, Torta DM, Sacco K, D'Agata F, Duca S, Geminiani G, Fox PT, Vercelli A, 2012a. Meta-analytic clustering of the insular cortex: characterizing the meta-analytic connectivity of the insula when involved in active tasks. *Neuroimage* 62, 343–355. [PubMed: 22521480]
- Cauda F, D'Agata F, Sacco K, Duca S, Geminiani G, Vercelli A, 2011. Functional connectivity of the insula in the resting brain. *Neuroimage* 55, 8–23. [PubMed: 21111053]
- Cauda F, Nani A, Costa T, Palermo S, Tatu K, Manuella J, Duca S, Fox PT, Keller R, 2018. The morphometric co-atrophy networking of schizophrenia, autistic and obsessive spectrum disorders. *Hum Brain Mapp*
- Cauda F, Torta DM, Sacco K, Geda E, D'Agata F, Costa T, Duca S, Geminiani G, Amanzio M, 2012b. Shared “core” areas between the pain and other task-related networks. *PLoS One* 7, e41929. [PubMed: 22900003]
- Chang LJ, Yarkoni T, Khaw MW, Sanfey AG, 2013. Decoding the role of the insula in human cognition: functional parcellation and large-scale reverse inference. *Cereb Cortex* 23, 739–749. [PubMed: 22437053]
- Christopher L, Koshimori Y, Lang AE, Criaud M, Strafella AP, 2014. Uncovering the role of the insula in non-motor symptoms of Parkinson's disease. *Brain* 137, 2143–2154. [PubMed: 24736308]
- Cole MW, Repovs G, Anticevic A, 2014. The frontoparietal control system: a central role in mental health. *Neuroscientist* 20, 652–664. [PubMed: 24622818]
- Cole MW, Schneider W, 2007. The cognitive control network: Integrated cortical regions with dissociable functions. *Neuroimage* 37, 343–360. [PubMed: 17553704]
- Craig AD, 2002. How do you feel? Interoception: the sense of the physiological condition of the body. *Nat Rev Neurosci* 3, 655–666. [PubMed: 12154366]
- Crossley NA, Mechelli A, Scott J, Carletti F, Fox PT, McGuire P, Bullmore ET, 2014. The hubs of the human connectome are generally implicated in the anatomy of brain disorders. *Brain* 137, 2382–2395. [PubMed: 25057133]
- Crossley NA, Scott J, Ellison-Wright I, Mechelli A, 2015. Neuroimaging distinction between neurological and psychiatric disorders. *Br J Psychiatry* 207, 429–434. [PubMed: 26045351]
- Eickhoff SB, Bzdok D, Laird AR, Kurth F, Fox PT, 2012. Activation likelihood estimation meta-analysis revisited. *Neuroimage* 59, 2349–2361. [PubMed: 21963913]
- Eickhoff SB, Laird AR, Fox PM, Lancaster JL, Fox PT, 2017. Implementation errors in the GingerALE Software: Description and recommendations. *Hum Brain Mapp* 38, 7–11. [PubMed: 27511454]
- Eickhoff SB, Laird AR, Grefkes C, Wang LE, Zilles K, Fox PT, 2009. Coordinate-based activation likelihood estimation meta-analysis of neuroimaging data: a random-effects approach based on empirical estimates of spatial uncertainty. *Hum Brain Mapp* 30, 2907–2926. [PubMed: 19172646]
- Esposito F, Goebel R, 2011. Extracting functional networks with spatial independent component analysis: the role of dimensionality, reliability and aggregation scheme. *Curr Opin Neurol* 24, 378–385. [PubMed: 21734575]
- Fox PT, Laird AR, Fox SP, Fox PM, Uecker AM, Crank M, Koenig SF, Lancaster JL, 2005. BrainMap taxonomy of experimental design: description and evaluation. *Hum Brain Mapp* 25, 185–198. [PubMed: 15846810]
- Fox PT, Lancaster JL, 2002. Opinion: Mapping context and content: the BrainMap model. *Nat Rev Neurosci* 3, 319–321. [PubMed: 11967563]
- Gejman PV, Sanders AR, Kendler KS, 2011. Genetics of schizophrenia: new findings and challenges. *Annu Rev Genomics Hum Genet* 12, 121–144. [PubMed: 21639796]
- Goodkind M, Eickhoff SB, Oathes DJ, Jiang Y, Chang A, Jones-Hagata LB, Ortega BN, Zaiko YV, Roach EL, Korgaonkar MS, Grieve SM, Galatzer-Levy I, Fox PT, Etkin A, 2015. Identification of a common neurobiological substrate for mental illness. *JAMA Psychiatry* 72, 305–315. [PubMed: 25651064]
- Hyman SE, 2010. The diagnosis of mental disorders: the problem of reification. *Annu Rev Clin Psychol* 6, 155–179. [PubMed: 17716032]

- Insel TR, 2014. The NIMH Research Domain Criteria (RDoC) Project: precision medicine for psychiatry. *Am J Psychiatry* 171, 395–397. [PubMed: 24687194]
- Iturria-Medina Y, Evans AC, 2015. On the central role of brain connectivity in neurodegenerative disease progression. *Front Aging Neurosci* 7, 90. [PubMed: 26052284]
- Kendler KS, Myers JM, Maes HH, Keyes CL, 2011. The relationship between the genetic and environmental influences on common internalizing psychiatric disorders and mental well-being. *Behav Genet* 41, 641–650. [PubMed: 21451959]
- Kendler KS, Prescott CA, Myers J, Neale MC, 2003. The structure of genetic and environmental risk factors for common psychiatric and substance use disorders in men and women. *Arch Gen Psychiatry* 60, 929–937. [PubMed: 12963675]
- Kessler RC, Demler O, Frank RG, Olfson M, Pincus HA, Walters EE, Wang P, Wells KB, Zaslavsky AM, 2005. Prevalence and treatment of mental disorders, 1990 to 2003. *N Engl J Med* 352, 2515–2523. [PubMed: 15958807]
- Krueger RF, 1999. The structure of common mental disorders. *Arch Gen Psychiatry* 56, 921–926. [PubMed: 10530634]
- Krueger RF, Markon KE, 2006. Reinterpreting comorbidity: a model-based approach to understanding and classifying psychopathology. *Annu Rev Clin Psychol* 2, 111–133. [PubMed: 17716066]
- Krueger RF, Markon KE, 2011. A dimensional-spectrum model of psychopathology: progress and opportunities. *Arch Gen Psychiatry* 68, 10–11. [PubMed: 21199961]
- Lahey BB, Van Hulle CA, Singh AL, Waldman ID, Rathouz PJ, 2011. Higher-order genetic and environmental structure of prevalent forms of child and adolescent psychopathology. *Arch Gen Psychiatry* 68, 181–189. [PubMed: 21300945]
- Laird AR, Fox PM, Price CJ, Glahn DC, Uecker AM, Lancaster JL, Turkeltaub PE, Kochunov P, Fox PT, 2005a. ALE meta-analysis: controlling the false discovery rate and performing statistical contrasts. *Hum Brain Mapp* 25, 155–164. [PubMed: 15846811]
- Laird AR, Lancaster JL, Fox PT, 2005b. BrainMap: the social evolution of a human brain mapping database. *Neuroinformatics* 3, 65–78. [PubMed: 15897617]
- Liloia D, Cauda F, Nani A, Manuella J, Duca S, Fox PT, Costa T, submitted. Negentropy maps as patterns of the pathological alteration specificity of brain regions. Data in brief
- Magurran AE, 2004. *Measuring Biological Diversity* Blackwell, Oxford.
- Manuella J, Nani A, Premi E, Borroni B, Costa T, Tatu K, Liloia D, Duca S, Cauda F, 2018. The Pathoconnectivity Profile of Alzheimer's Disease: A Morphometric Coalteration Network Analysis. *Front Neurol* 8.
- Markon KE, 2010. Modeling psychopathology structure: a symptom-level analysis of Axis I and II disorders. *Psychol Med* 40, 273–288. [PubMed: 19515267]
- McTeague LM, Goodkind MS, Etkin A, 2016. Transdiagnostic impairment of cognitive control in mental illness. *J Psychiatr Res* 83, 37–46. [PubMed: 27552532]
- Miyake A, Friedman NP, 2012. The Nature and Organization of Individual Differences in Executive Functions: Four General Conclusions. *Curr Dir Psychol Sci* 21, 8–14. [PubMed: 22773897]
- Mohan A, Roberto AJ, Mohan A, Lorenzo A, Jones K, Carney MJ, Liogier-Weyback L, Hwang S, Lapidus KA, 2016. The Significance of the Default Mode Network (DMN) in Neurological and Neuropsychiatric Disorders: A Review. *Yale J Biol Med* 89, 49–57. [PubMed: 27505016]
- Padovani A, Premi E, Pilotto A, Gazzina S, Cosseddu M, Archetti S, Cancelli V, Paghera B, Borroni B, 2013. Overlap between frontotemporal dementia and Alzheimer's disease: cerebrospinal fluid pattern and neuroimaging study. *J Alzheimers Dis* 36, 49–55. [PubMed: 23568100]
- Plomin R, Haworth CM, Davis OS, 2009. Common disorders are quantitative traits. *Nat Rev Genet* 10, 872–878. [PubMed: 19859063]
- Purcell SM, Wray NR, Stone JL, Visscher PM, O'Donovan MC, Sullivan PF, Sklar P, 2009. Common polygenic variation contributes to risk of schizophrenia and bipolar disorder. *Nature* 460, 748–752. [PubMed: 19571811]
- Raj A, Kuceyeski A, Weiner M, 2012. A network diffusion model of disease progression in dementia. *Neuron* 73, 1204–1215. [PubMed: 22445347]

- Seeley WW, Crawford RK, Zhou J, Miller BL, Greicius MD, 2009. Neurodegenerative diseases target large-scale human brain networks. *Neuron* 62, 42–52. [PubMed: 19376066]
- Shannon CE, 1948. A mathematical theory of communication. *The Bell System Technical Journal* 27, 379–423.
- Singer T, Critchley HD, Preuschoff K, 2009. A common role of insula in feelings, empathy and uncertainty. *Trends Cogn Sci* 13, 334–340. [PubMed: 19643659]
- Tatu K, Costa T, Nani A, Diano M, Quarta DG, Duca S, Apkarian AV, Fox PT, Cauda F, 2018. How do morphological alterations caused by chronic pain distribute across the brain? A meta-analytic co-alteration study. *NeuroImage: Clinical* 18, 15–30. [PubMed: 30023166]
- Turkeltaub PE, Eickhoff SB, Laird AR, Fox M, Wiener M, Fox P, 2012. Minimizing within-experiment and within-group effects in Activation Likelihood Estimation meta-analyses. *Hum Brain Mapp* 33, 1–13. [PubMed: 21305667]
- Vanasse TJ, Fox PM, Barron DS, Robertson M, Eickhoff SB, Lancaster JL, Fox PT, 2018. BrainMap VBM: An environment for structural meta-analysis. *Hum Brain Mapp*
- Vercelli U, Diano M, Costa T, Nani A, Duca S, Geminiani G, Vercelli A, Cauda F, 2016. Node Detection Using High-Dimensional Fuzzy Parcellation Applied to the Insular Cortex. *Neural Plast* 2016, 1938292. [PubMed: 26881093]
- Wen W, Thalamuthu A, Mather KA, Zhu W, Jiang J, de Micheaux PL, Wright MJ, Ames D, Sachdev PS, 2016. Distinct Genetic Influences on Cortical and Subcortical Brain Structures. *Sci Rep* 6, 32760. [PubMed: 27595976]
- World Health Organization, 2007. *International Classification of Diseases* World Health Organization, Geneva.
- Zhou J, Gennatas ED, Kramer JH, Miller BL, Seeley WW, 2012. Predicting regional neurodegeneration from the healthy brain functional connectome. *Neuron* 73, 1216–1227. [PubMed: 22445348]

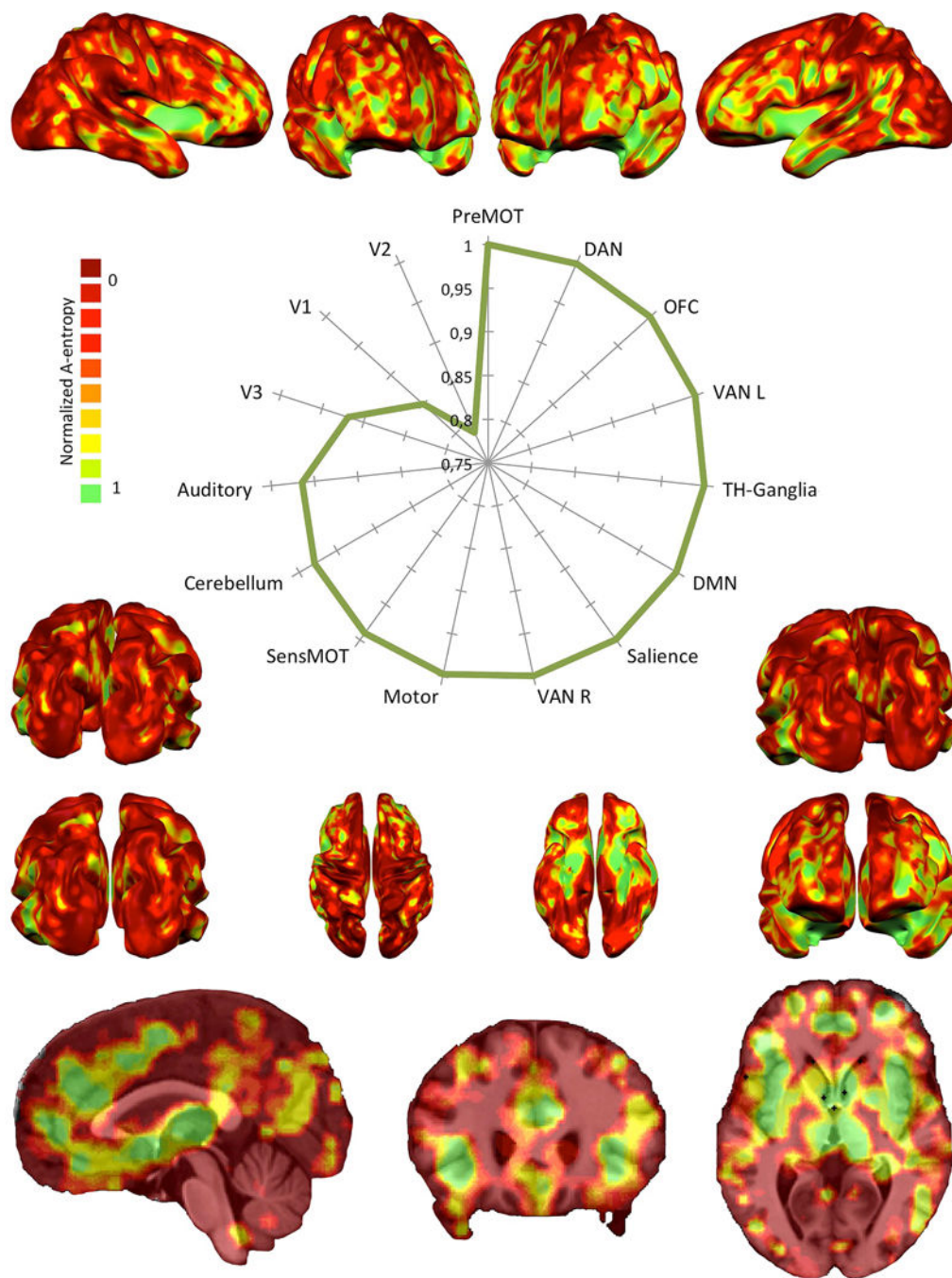


**Figure 1.** 2D and 3D (fine-grained) visualizations of disease-related alteration entropy maps. The radar graph illustrates the mean alteration entropy values of the principal large-scale brain networks: premotor (PreMOT), dorsal attentional (DAN), ventral attentional right and left (VAN R and L), thalamus and basal ganglia (TH-Ganglia), default mode network (DMN), salience network (Saliency), motor network (Motor), sensorimotor network (SensMOT), Cerebellum, auditory network (Auditory), visual network (V1, V2, V3).

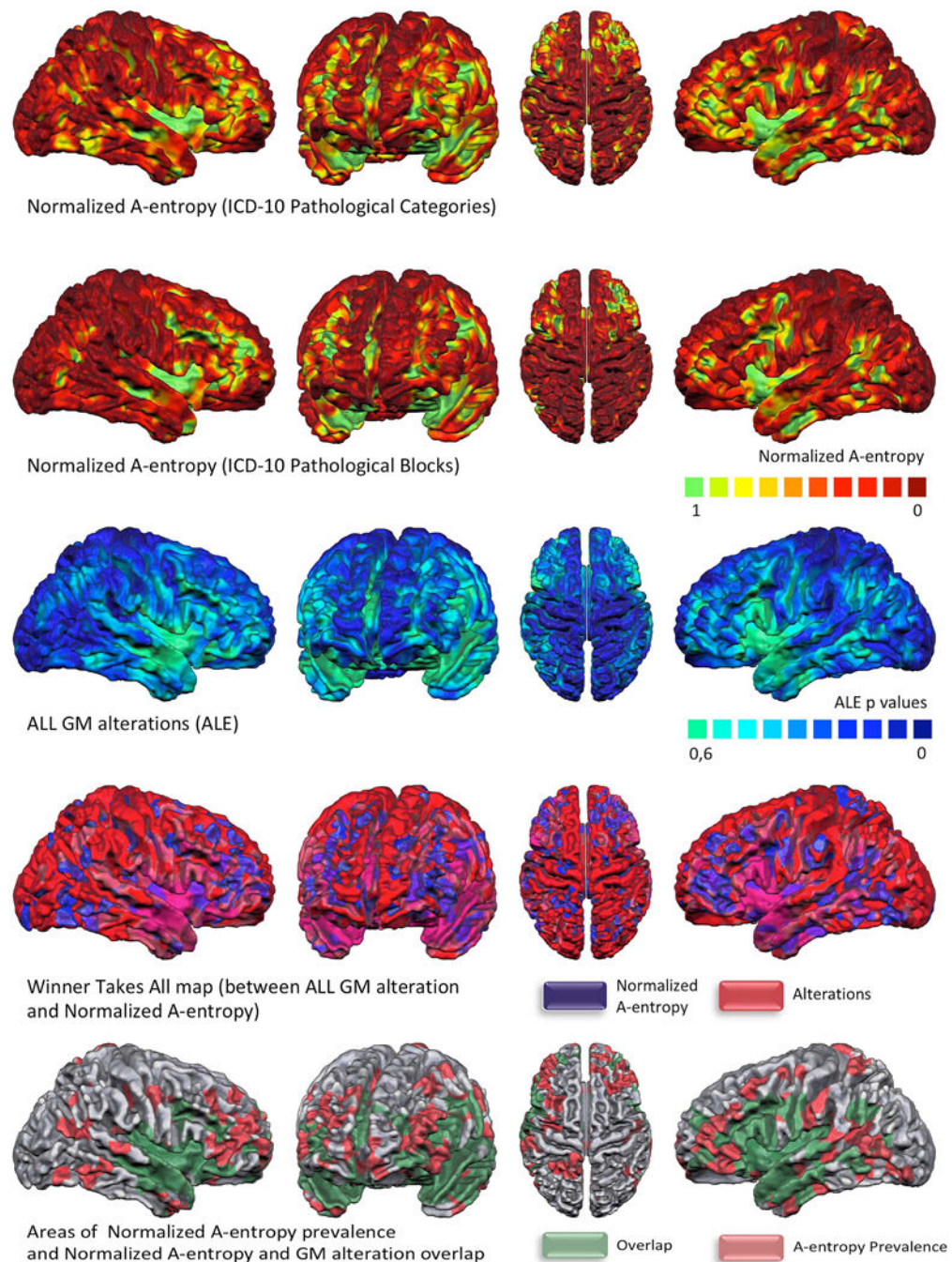


**Figure 2.**

Comparison between the alteration entropy calculated on the basis of a fine-grained neuropathological subdivision (ICD pathological categories, upper panel first row) and the alteration entropy calculated on the basis of a coarser subdivision (ICD pathological blocks, upper panel second row). The middle panel illustrates a map of the probability for each brain area to be altered (derived from an unthresholded ALE map of all the disease-related gray matter (GM) alterations detected with VBM and included in the BrainMap database). The lower panel (row before the last) shows a winner takes all (WTA) comparison between the

ALE map and the A-entropy map (fine-grained). Regions showing a prevalence of the A-entropy values (i.e., with high A-entropy values but less frequently altered) are highlighted in blue. Regions showing a prevalence of the ALE values (frequently altered but proportionally with lower A-entropy values) are highlighted in blue. The lower panel (last row) shows a comparison between the thresholded ALE map and the A-entropy map (fine-grained, thresholded to show only the voxels with values  $>0.5$ ). Regions with high A-entropy values but not frequently altered (and thereby not overlapping with significant areas in the ALE map) are highlighted in red. Regions with both high A-entropy and significant ALE values are highlighted in green. No areas with significant ALE values and low A-entropy were found. All the significant ALE values characterize areas that also show high A-entropy.

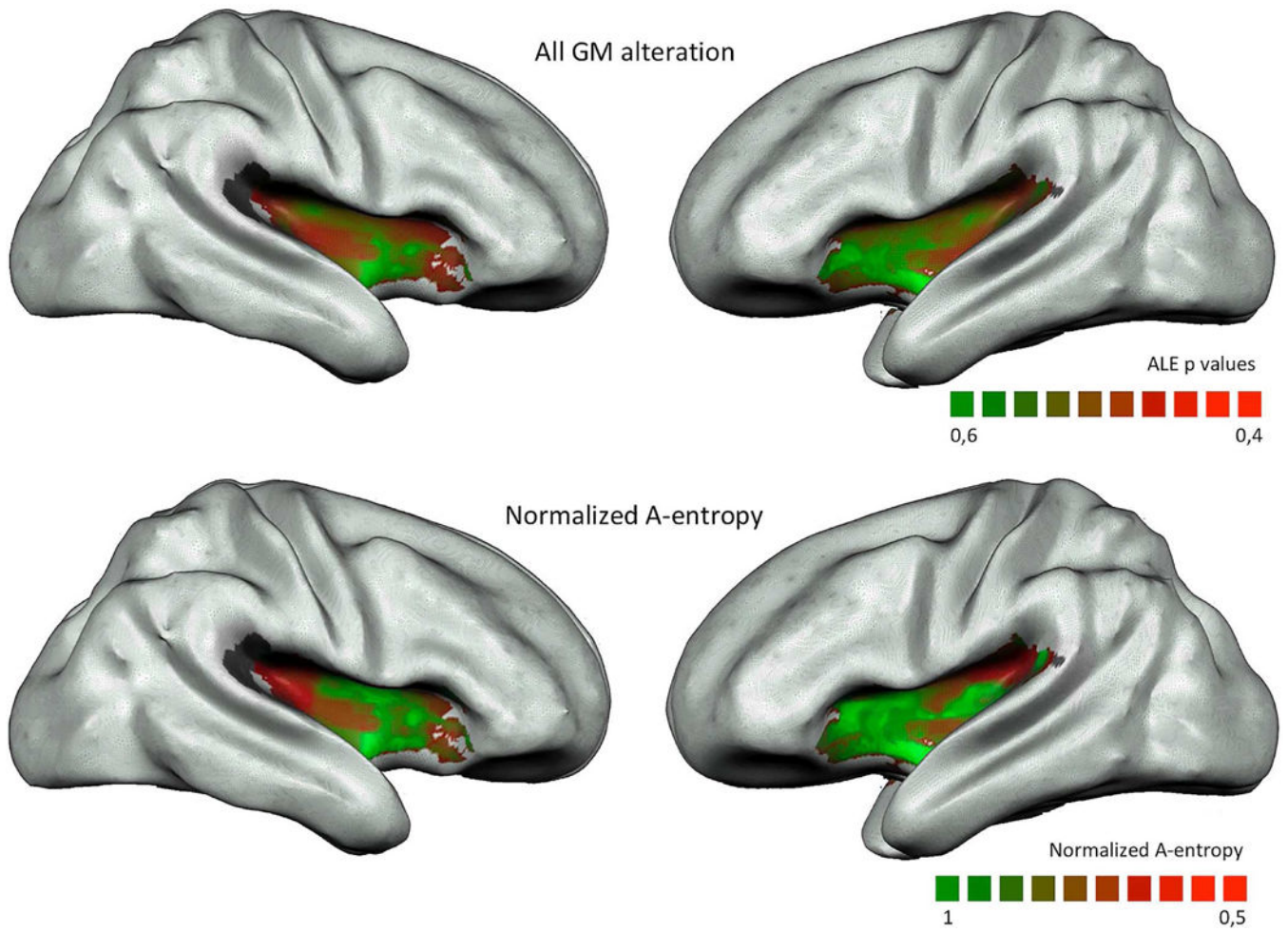


**Figure 3.** Comparison between the insular areas that were most frequently reported as being altered in our sample (upper panels) and the brain areas showing the highest A-entropy values (lower panels).

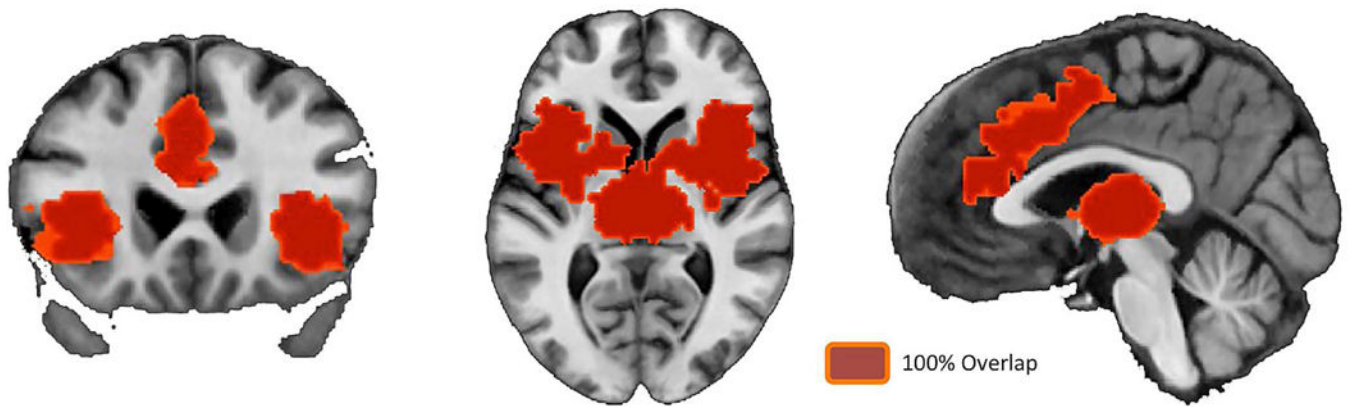


**Figure 4.** Bidimensional view of the areas exhibiting 100% of overlap between the thresholded ALE map of the most frequently altered brain regions and the A-entropy map (50% of the regions having the highest A-entropy values).

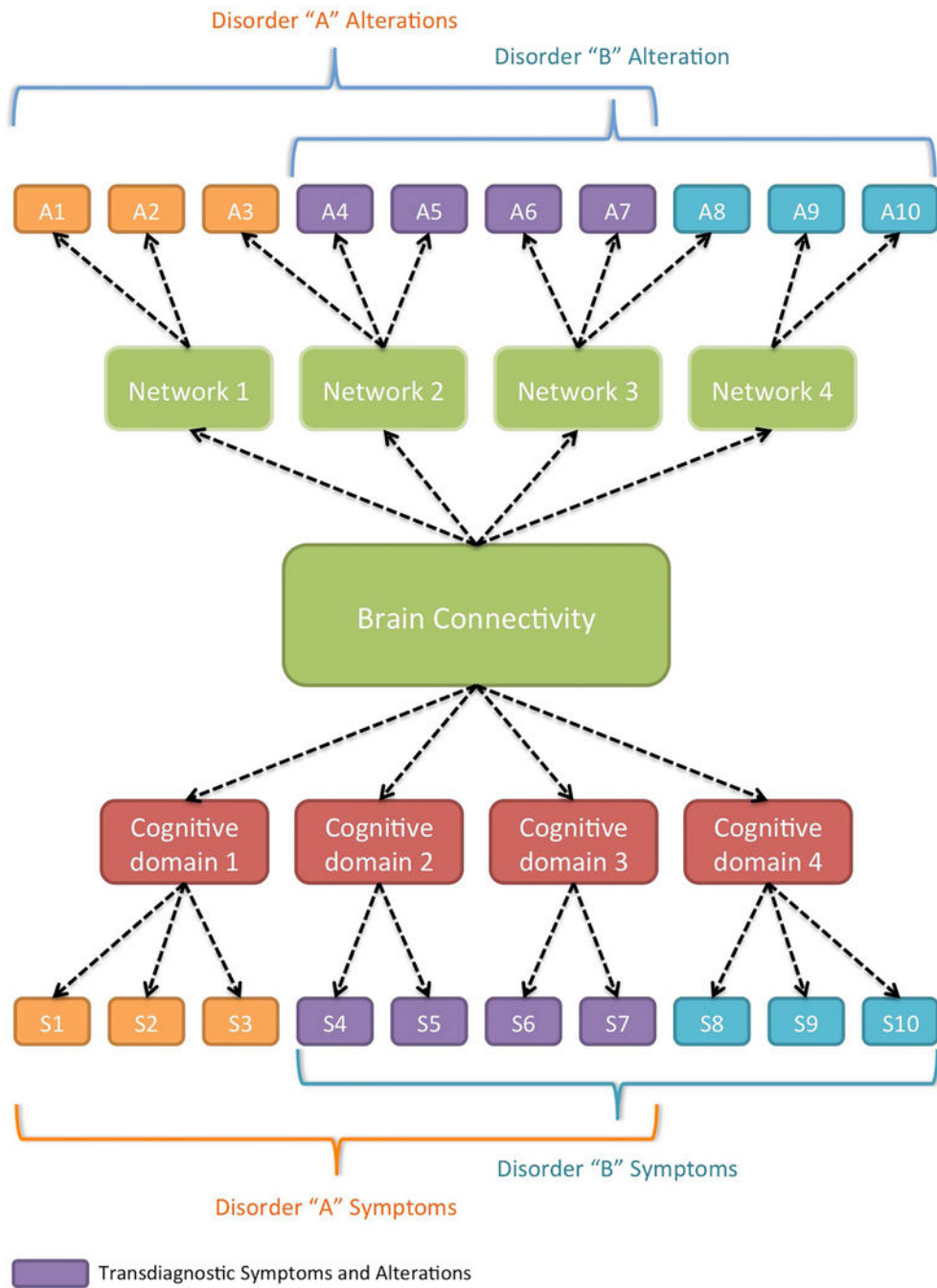


**Figure 5.** Diagram depicting the model proposed by Buckholtz and Meyer-Lindenberg (2012).

**Table 1.**

Local Maxima normalized alteration entropy values, mean normalized alteration entropy values and Talairach coordinates of the different brain areas.

ID	Brain Area	Local Maxima (Talairach)			Maximum Normalized Entropy	Mean Normalized Entropy
		X	Y	Z		
1	Right Anterior Insula (BA 13)	30	18	-3	0,999	0,327
2	Left Precentral Gyrus (BA 6)	-51	0	35	0,999	0,221
3	Left Inferior Temporal Gyrus (BA 20)	-57	-27	-18	0,999	0,448
4	Left Middle Frontal Gyrus (BA 10)	-39	48	12	0,999	0,304
5	Right Anterior Insula (BA 13)	33	16	0	0,999	0,816
6	Right Insula (BA 45)	30	24	3	0,999	0,194
7	Left Medial Frontal Gyrus (BA 9)	-6	36	30	0,999	0,355
8	Right Caudate Head	6	3	-3	0,999	0,759
9	Left Middle Frontal Gyrus (BA 46)	-40	48	15	0,999	0,237
10	Right Anterior Cingulate (BA 25)	4	3	-6	0,999	0,517
11	Right Anterior Cingulate (BA 32)	3	36	21	0,998	0,544
12	Left Inferior Frontal Gyrus (BA 47)	-36	24	0	0,998	0,354
13	Right Superior Temporal Gyrus (BA 38)	33	18	-21	0,998	0,268
14	Right Anterior Cingulate (BA 10)	6	48	6	0,998	0,284
15	Left Cingulate Gyrus (BA 32)	-4	36	29	0,998	0,552
16	Right Posterior Insula (BA 13)	42	-9	3	0,998	0,535
17	Right Parahippocampal Gyrus (BA 34)	30	3	-18	0,998	0,845
18	Left Parahippocampal Gyrus (BA 35)	-24	-15	-21	0,998	0,804
19	Right Parahippocampal Gyrus (BA 35)	24	-24	-14	0,998	0,702
20	Left Anterior Insula (BA 13)	-39	3	6	0,998	0,869
21	Right Amygdala	18	-6	-21	0,997	0,954
22	Left Middle Temporal Gyrus (BA 21)	-55	-18	-15	0,997	0,339
23	Right Pulvinar	4	-24	10	0,997	0,684
24	Left Superior Temporal Gyrus (BA 41)	-48	-33	12	0,997	0,582
25	Left Uncus (BA 28)	-27	-12	-25	0,997	0,789
26	Right Anterior Cingulate (BA 24)	1	27	23	0,997	0,277
27	Left Parahippocampal Gyrus (BA 34)	-21	-12	-18	0,996	0,839
28	Right Middle Temporal Gyrus (BA 21)	48	6	-33	0,996	0,279
29	Left Hippocampus	-26	-12	-22	0,996	0,894
30	Left Caudate Head	-6	12	-6	0,996	0,817
31	Right Medial Frontal Gyrus (BA 9)	1	36	30	0,996	0,299
32	Left Pulvinar	-6	-24	9	0,995	0,707
33	Left Anterior Cingulate (BA 24)	-3	21	-6	0,995	0,266
34	Left Amygdala	-21	-9	-18	0,995	0,975

ID	Brain Area	Local Maxima (Talairach)			Maximum Normalized Entropy	Mean Normalized Entropy
		X	Y	Z		
35	Left Superior Temporal Gyrus (BA 42)	-54	-34	18	0,995	0,281
36	Right Anterior Nucleus (Thalamus)	9	-12	15	0,995	0,663
37	Left Posterior Insula (BA 13)	-40	0	8	0,995	0,445
38	Left Precentral Gyrus (BA 44)	-41	6	6	0,994	0,317
39	Left Medial Dorsal Nucleus (Thalamus)	-6	-23	9	0,994	0,941
40	Right Caudate Body	9	12	9	0,993	0,534
41	Right Precentral Gyrus (BA 44)	42	12	6	0,993	0,365
42	Right Medial Dorsal Nucleus (Thalamus)	3	-21	6	0,993	0,940
43	Left Medial Frontal Gyrus (BA 11)	-5	36	-12	0,993	0,125
44	Left Medial Globus Pallidus	-8	0	0	0,993	0,499
45	Left Superior Temporal Gyrus (BA 22)	-48	12	-6	0,991	0,291
46	Left Inferior Frontal Gyrus (BA 45)	-36	24	2	0,991	0,214
47	Left Lateral Globus Pallidus	-24	-6	-3	0,991	0,512
48	Left Putamen	-24	-6	-3	0,991	0,576
49	Right Precentral Gyrus (BA 4)	48	-12	42	0,990	0,160
50	Left Caudate Body	-9	6	9	0,990	0,596
51	Left Lateral Posterior Nucleus (Thalamus)	-18	-21	9	0,990	0,759
52	Left Parahippocampal Gyrus (BA 36)	-28	-15	-24	0,989	0,603
53	Right Hippocampus	27	-22	-12	0,988	0,835
54	Right Medial Frontal Gyrus (BA 6)	2	36	33	0,987	0,185
55	Right Parahippocampal Gyrus (BA 36)	24	-29	-12	0,987	0,510
56	Right Hypothalamus	4	-1	-6	0,984	0,599
57	Left Precentral Gyrus (BA 4)	-36	-13	52	0,983	0,206
58	Right Medial Frontal Gyrus (BA 11)	1	36	-11	0,982	0,076
59	Right Supramarginal Gyrus (BA 40)	54	-53	27	0,980	0,182
60	Right Cerebellar Tonsil	12	-45	-42	0,980	0,037
61	Right Midline Nucleus (Thalamus)	7	-15	15	0,979	0,942
62	Right Putamen	27	-9	9	0,979	0,584
63	Right Superior Temporal Gyrus (BA 39)	54	-54	27	0,977	0,140
64	Left Mammillary Body	-8	-18	3	0,976	0,570
65	Right Posterior Cingulate (BA 29)	3	-57	9	0,975	0,329
66	Left Parahippocampal Gyrus (BA 37)	-30	-39	-12	0,973	0,334
67	Right Superior Temporal Gyrus (BA 22)	45	-21	0	0,970	0,285
68	Right Ventral Lateral Nucleus (Thalamus)	11	-12	15	0,969	0,677
69	Right Mammillary Body	8	-21	5	0,968	0,470
70	Right Fusiform Gyrus (BA 37)	30	-36	-12	0,968	0,323
71	Right Lateral Dorsal Nucleus (Thalamus)	10	-16	15	0,968	0,869
72	Left Midline Nucleus (Thalamus)	-7	-20	14	0,968	0,903

ID	Brain Area	Local Maxima (Talairach)			Maximum Normalized Entropy	Mean Normalized Entropy
		X	Y	Z		
73	Left Hypothalamus	-5	-3	-5	0,963	0,648
74	Left Middle Frontal Gyrus (BA 8)	-30	39	39	0,962	0,175
75	Right Postcentral Gyrus (BA 3)	48	-15	42	0,958	0,179
76	Right Middle Frontal Gyrus (BA 46)	42	31	22	0,957	0,171
77	Left Postcentral Gyrus (BA 3)	-54	-15	30	0,957	0,144
78	Right Parahippocampal Gyrus (BA 27)	24	-30	-7	0,955	0,448
79	Left Postcentral Gyrus (BA 40)	-57	-27	21	0,954	0,151
80	Left Ventral Lateral Nucleus (Thalamus)	-6	-9	6	0,952	0,758
81	Right Medial Globus Pallidus	9	3	-3	0,948	0,523
82	Left Lateral Dorsal Nucleus (Thalamus)	-9	-20	14	0,948	0,883
83	Right Red Nucleus	4	-20	2	0,947	0,209
84	Right Postcentral Gyrus (BA 2)	48	-24	42	0,944	0,233
85	Right Superior Temporal Gyrus (BA 41)	54	-24	14	0,943	0,340
86	Right Lateral Globus Pallidus	18	0	-7	0,943	0,466
87	Left Anterior Nucleus (Thalamus)	-6	-9	12	0,939	0,748
88	Left Medial Geniculus Body	-15	-24	2	0,935	0,534
89	Right Declive (Cerebellum)	15	-60	-12	0,933	0,157
90	Right Ventral Posterior Medial Nucleus (Thalamus)	12	-19	10	0,932	0,589
91	Right Nucleus Accumbens	9	12	-6	0,931	0,789
92	Right Lateral Posterior Nucleus (Thalamus)	13	-22	12	0,931	0,573
93	Right Medial Frontal Gyrus (BA 8)	3	42	42	0,930	0,291
94	Right Cuneus (BA 18)	3	-87	24	0,922	0,134
95	Left Precuneus (BA 7)	-3	-63	36	0,921	0,236
96	Left Ventral Anterior Nucleus (Thalamus)	-6	-7	3	0,919	0,493
97	Left Middle Occipital Gyrus (BA 18)	-36	-81	-9	0,919	0,104
98	Right Ventral Posterior Lateral Nucleus (Thalamus)	12	-16	10	0,918	0,488
99	Left Middle Temporal Gyrus (BA 39)	-51	-57	9	0,916	0,240
100	Right Inferior Temporal Gyrus (BA 20)	36	-6	-36	0,916	0,311
101	Left Postcentral Gyrus (BA 2)	-54	-19	30	0,915	0,200
102	Left Declive (Cerebellum)	-42	-69	-18	0,914	0,129
103	Left Middle Occipital Gyrus (BA 19)	-54	-60	-6	0,912	0,128
104	Right Caudate Tail	36	-16	-6	0,912	0,353
105	Left Caudate Tail	-36	-14	-10	0,910	0,370
106	Left Precuneus (BA 31)	-9	-54	30	0,907	0,272

ID	Brain Area	Local Maxima (Talairach)			Maximum Normalized Entropy	Mean Normalized Entropy
		X	Y	Z		
107	Right Cuneus (BA 19)	3	-87	25	0,907	0,170
108	Left Nucleus Accumbens	-9	13	-8	0,906	0,503
109	Left Posterior Cingulate (BA 23)	-6	-39	27	0,906	0,246
110	Right Precuneus (BA 7)	0	-60	36	0,904	0,160
111	Right Cingulate Gyrus (BA 23)	0	-33	27	0,904	0,275
112	Left Culmen (Cerebellum)	-24	-33	-18	0,901	0,064
113	Right Culmen (Cerebellum)	12	-63	-10	0,901	0,095
114	Left Tuber (Cerebellum)	-42	-69	-23	0,900	0,076
115	Right Superior Temporal Gyrus (BA 42)	57	-30	6	0,899	0,163
116	Left Parahippocampal Gyrus (BA 27)	-24	-34	-3	0,896	0,533
117	Right Cingulate Gyrus (BA 31)	6	-57	30	0,895	0,300
118	Left Parahippocampal Gyrus (BA 30)	-18	-42	-3	0,895	0,175
119	Right Ventral Anterior Nucleus (Thalamus)	12	-9	12	0,885	0,469
120	Left Inferior Semi-Lunar Lobule (Cerebellum)	-24	-66	-39	0,881	0,043
121	Right Tuber (Cerebellum)	33	-57	-30	0,876	0,045
122	Left Cerebellar Tonsil	-24	-63	-45	0,876	0,044
123	Right Pyramis (Cerebellum)	29	-57	-30	0,876	0,097
124	Right Inferior Semi-Lunar Lobule (Cerebellum)	24	-78	-35	0,876	0,027
125	Left Precentral Gyrus (BA 43)	-57	-6	12	0,876	0,228
126	Left Red Nucleus	-7	-18	2	0,863	0,146
127	Left Postcentral Gyrus (BA 1)	-56	-25	37	0,857	0,073
128	Right Lateral Geniculum Body	24	-26	-3	0,856	0,194
129	Left Paracentral Lobule (BA 5)	-9	-42	60	0,842	0,178
130	Right Uvula (Cerebellum)	20	-73	-31	0,838	0,057

ID	Brain Area	Local Maxima (Talairach)			Maximum Normalized Entropy	Mean Normalized Entropy
		X	Y	Z		
13 1	Right Anterior Cingulate (BA 33)	1	22	22	0,824	0,280
13 2	Right Precentral Gyrus (BA 43)	54	-3	12	0,803	0,213
13 3	Left Lingual Gyrus (BA 17)	-4	-84	1	0,784	0,050
13 4	Medulla Oblongata	3	-39	-42	0,778	0,071
13 5	Left Cerebellar Lingual	-6	-45	-18	0,777	0,152
13 6	Right Postcentral Gyrus (BA 1)	62	-23	34	0,776	0,095
13 7	Left Fastigium (Cerebellum)	-6	-47	-19	0,762	0,180
13 8	Right Postcentral Gyrus (BA 5)	6	-46	63	0,755	0,170
13 9	Left Anterior Cingulate (BA 33)	-3	22	21	0,753	0,203
14 0	Left Lateral Geniculus Body	-24	-27	-3	0,748	0,343
14 1	Left Subthalamic Nucleus	-11	-11	2	0,742	0,183
14 2	Left Posterior Cingulate (BA 29)	-6	-41	22	0,741	0,078
14 3	Right Culmen (Cerebellum)	5	-33	-13	0,700	0,074
14 4	Left Substantia Nigra	-17	-20	-6	0,625	0,074
14 5	Right Pons	14	-14	-19	0,572	0,015
14 6	Left Lingual Gyrus (BA 17)	0	-84	3	0,560	0,092
14 7	Right Subthalamic Nucleus	11	-12	2	0,540	0,106
14 8	Left Dentate (Cerebellum)	-12	-47	-18	0,487	0,031
14 9	Right Medial Geniculus Body	14	-24	2	0,475	0,073
15 0	Left Declive (Cerebellum)	0	-75	-12	0,317	0,028
15 1	Right Dentate (Cerebellum)	18	-54	-18	0,317	0,012
15 2	Left Nodule (Cerebellum)	-6	-46	-26	0,218	0,004
15 3	Right Substantia Nigra	16	-20	-6	0,214	0,019
15 4	Right Fastigium (Cerebellum)	6	-48	-19	0,212	0,019

<i>ID</i>	<i>Brain Area</i>	<i>Local Maxima (Talairach)</i>			<i>Maximum Normalized Entropy</i>	<i>Mean Normalized Entropy</i>
		<i>X</i>	<i>Y</i>	<i>Z</i>		
15 5	Right Culmen (Cerebellum)	6	-59	3	0,206	0,011
15 6	Left Uvula (Cerebellum)	-4	-60	-34	0,164	0,006
15 7	Left Tuber (Cerebellum)	-1	-75	-24	0,093	0,009
15 8	Right Locus Coeruleus	6	-28	-8	0,037	0,006
15 9	Left Pyramis (Cerebellum)	-2	-78	-27	0,026	0,003
16 0	Left Locus Coeruleus	-5	-25	-7	0,013	0,004

Author Manuscript

Author Manuscript

Author Manuscript

Author Manuscript